

# Electronic excited states in deep variational Monte Carlo

M. T. Entwistle,<sup>1,\*</sup> Z. Schätzle,<sup>1,\*</sup> P. A. Erdman,<sup>1</sup> J. Hermann,<sup>1,†</sup> and F. Noé<sup>1,2,3,4,‡</sup>

<sup>1</sup>*FU Berlin, Department of Mathematics and Computer Science, Arnimallee 12, 14195 Berlin, Germany*

<sup>2</sup>*FU Berlin, Department of Physics, Arnimallee 14, 14195 Berlin, Germany*

<sup>3</sup>*Rice University, Department of Chemistry, Houston, Texas 77005, USA*

<sup>4</sup>*Microsoft Research Cambridge, United Kingdom*

(Dated: March 18, 2022)

Obtaining accurate ground and low-lying excited states of electronic systems is crucial in a multitude of important applications. One *ab initio* method for solving the electronic Schrödinger equation that scales favorably for large systems and whose accuracy is limited only by the choice of wavefunction ansatz employed is variational quantum Monte Carlo (QMC). The recently introduced deep QMC approach, using a new class of ansatzes represented by deep neural networks, has been shown to generate nearly exact ground-state solutions for molecules containing up to a few dozen electrons, with the potential to scale to much larger systems where other highly accurate methods are not feasible. In this paper, we advance one such ansatz (PauliNet) to compute electronic excited states through a simple variational procedure. We demonstrate our method on a variety of small atoms and molecules where we consistently achieve high accuracy for low-lying states. To highlight the method’s potential for larger systems, we show that for the benzene molecule, PauliNet is on par with significantly more expensive high-level electronic structure methods in terms of the excitation energy and outperforms them in terms of absolute energies.

## I. INTRODUCTION

The fundamental challenge of quantum chemistry, solid-state physics and many areas of computational materials science is to obtain solutions to the electronic Schrödinger equation for a given system, which in principle provide complete access to its chemical properties. The ground and low-lying excited states typically determine the behavior of a system at typical *in vitro* and *in vivo* conditions and are therefore of the most interest in many applications. Understanding and being able to describe excited-state processes [1], including a wide variety of important spectroscopy methods such as fluorescence, photoionization and optical absorption of molecules and solids, is key to the successful design of new materials.

Unfortunately, the Schrödinger equation cannot be solved exactly except in the simplest cases, such as one-dimensional toy systems or a single hydrogen atom. Accordingly, many approximate numerical methods have been developed which provide solutions at varying degrees of accuracy. Time-dependent density functional theory [2, 3] (TDDFT) is the most popular method due to its computational efficiency, but has well known limitations [4–9]. Higher-accuracy methods have a computational cost that scales rapidly with system size — the well known full configuration interaction [10] (FCI) and coupled cluster [11] (CC) techniques scale  $\sim \mathcal{O}(\exp(N))$  [12] and  $\sim \mathcal{O}(N^{5-10})$  [13] respectively, where  $N$  is the number of electrons, thereby severely limiting their practical use. There is thus a huge need for *ab initio* methods

that scale more favorably with system size, allowing the modeling of practically relevant molecules and materials.

Quantum Monte Carlo (QMC) techniques offer a route forward with their favorable scaling ( $\mathcal{O}(N^{3-4})$ ) and therefore dominate high-accuracy calculations where other methods are too expensive [14, 15]. A state-of-the-art QMC calculation typically involves the construction of a multi-determinant baseline wavefunction through standard electronic-structure methods, which is augmented with a Jastrow factor to efficiently incorporate electron correlation, and then optimized through variational QMC (VMC) to obtain a trial wavefunction. This is then used within fixed-node diffusion QMC (DMC) to obtain a final electronic energy. The fixed-node approximation is used to avoid exponential scaling, with the drawback that the nodal surface of the trial wavefunction cannot be modified, which limits the accuracy of the DMC result [16]. A more expressive baseline wavefunction can improve upon this but DMC often needs thousands to hundreds of thousands of determinants to reach convergence [17]. Additionally, DMC only provides the final energy, restricting the calculation of other electronic properties [18]. Both of these limitations can, in principle, be resolved at the VMC level, with its accuracy constrained only by the flexibility of the trainable wavefunction ansatz. So far, these techniques have mostly been developed for ground-state calculations, with different extensions proposed to address excited states [14, 19–28].

Recently the new *ab initio* approach of deep VMC methods has been introduced [29–32] and subsequently further extended and improved [33–35]. In particular, PauliNet [29] and FermiNet [30] were the first methods to demonstrate that highly accurate ground-state results for molecules could be obtained using deep VMC with a lower computational complexity and using orders of

\* M. T. Entwistle and Z. Schätzle contributed equally to this work.

† jan.hermann@fu-berlin.de

‡ frank.noé@fu-berlin.de

magnitude less Slater determinants typically employed in other methods that achieve similar accuracy.

In the same spirit as Carleo and Troyer proposed for optimizing quantum states in lattice models [36], VMC is used in order to train a neural network model that represents the many-body wavefunction in an unsupervised fashion, i.e. in contrast to other quantum machine learning approaches the only input to the method is the Hamiltonian, and training data are generated on the fly by sampling from the current wavefunction model and minimizing the variational energy. In both PauliNet and FermiNet deep antisymmetric neural networks are used to represent the fermionic wavefunction in the real space of electron coordinates.

Recently, there has been a lot of interest in developing deep learning methods for excited states [37]. In this paper, we extend PauliNet towards the *ab initio* computation of electronic excited states. The input is again only the Hamiltonian of the quantum system. By employing a simple energy minimization and numerical orthogonalization procedure, we are able to obtain the lowest excited-state wavefunctions of a given system. The excited-state optimization makes use of a penalty method that minimizes the overlap between the  $n$ -th excited state and the lower-lying states in the spectrum. Optimization methods that introduce additional constraints have been used in the context of VMC before [28] and provide a simple way to obtain orthogonal states without explicit enforcement in the wavefunction ansatzes. Combining these techniques with the expressiveness of neural network ansatzes yields highly accurate approximations to excited states with direct access to the wavefunctions for the evaluation of electronic observables.

We demonstrate our method on a variety of small- and medium-sized molecules, where we consistently achieve highly accurate total energies, outperforming traditional quantum chemistry methods. We also compute excitation energies, transition dipole moments and oscillator strengths, the main ground-to-excited transition properties, with the latter two known to be more sensitive to errors in the underlying wavefunctions than energies. In all test systems we find PauliNet closely matches high-order CC and experimental results. Finally, we show that our method can be applied in a straightforward manner to larger molecules, using the example of benzene where we match significantly more expensive high-level electronic structure methods in terms of the excitation energy and outperform them in terms of absolute energies.

## II. THEORY AND METHODS

### A. PauliNet ansatz

At the heart of our approach is the PauliNet ansatz, introduced in [29] and further refined in [38], a multi-determinant Slater-Jastrow-backflow type trial wave-

function which is parametrized by highly expressive deep neural networks:

$$\psi_{\theta}(\mathbf{r}) = e^{\gamma(\mathbf{r}) + J_{\theta}(\mathbf{r})} \sum_p c_p \det[\tilde{\varphi}_{\theta, \mu_p i}^{\uparrow}(\mathbf{r})] \det[\tilde{\varphi}_{\theta, \mu_p i}^{\downarrow}(\mathbf{r})], \quad (1)$$

$$\tilde{\varphi}_{\theta, \mu i}(\mathbf{r}) = \varphi_{\mu}(\mathbf{r}_i) f_{\theta, \mu i}^{(m)}(\mathbf{r}) + f_{\theta, \mu i}^{(a)}(\mathbf{r}), \quad (2)$$

where  $\mathbf{r} = (\mathbf{r}_1, \dots, \mathbf{r}_N)$  is the  $3N$ -dimensional real space of electron coordinates. The structure of our ansatz ensures that the correct physics is encoded: the wavefunction obeys exact asymptotic behavior through the fixed electronic cusps  $\gamma$ , and is antisymmetric with respect to the exchange of like-spin electrons through the use of Slater determinants of single-electron orbitals  $\varphi_{\mu}$ , thereby guaranteeing the Pauli exclusion principle is obeyed.

The expressiveness of PauliNet is contained in the Jastrow factor  $J_{\theta}$  and backflow  $\mathbf{f}_{\theta}$ , which introduce many-body correlation, and are both represented through deep neural networks (denoted by trainable parameters  $\theta$ ).  $J_{\theta}$  and  $\mathbf{f}_{\theta}$  are constructed in ways that preserve the antisymmetry of the fermionic wavefunction with respect to exchanging equal-spin electrons, as well as its cusp behavior. The Jastrow factor is an exchange-symmetric function, and captures complex correlation effects through augmenting the Slater determinant baseline, but is incapable of modifying the nodal surface of the determinant expansion. Changes to the nodal surface are possible through the backflow, which acts on the single-electron orbitals  $\varphi_{\mu}$  directly, transforming them into many-electron orbitals  $\tilde{\varphi}_{\mu}$ , and is designed to be equivariant under the exchange of like-spin electrons.

### B. Ground-state optimization

Like traditional VMC methods, PauliNet is based on the variational principle, which guarantees that the energy expectation value of a trial wavefunction  $\psi_{\theta}$  is an upper bound to the true ground-state energy:

$$E_0 = \min_{\psi} \langle \psi | \hat{H} | \psi \rangle \leq \min_{\theta} \langle \psi_{\theta} | \hat{H} | \psi_{\theta} \rangle. \quad (3)$$

For a given system, a standard quantum chemistry method (Hartree-Fock (HF) for a single determinant; complete active space self-consistent field (CASSCF) for multiple determinants) is performed, with the solution supplemented by the analytically known cusp conditions, thus producing a reasonable baseline wavefunction. We then optimize the PauliNet ansatz by minimizing the total electronic energy (serving directly as the loss), following the standard VMC trick of evaluating it as an expectation value of the local energy,  $E_{\text{loc}}(\mathbf{r}) = \hat{H}\psi(\mathbf{r})/\psi(\mathbf{r})$ :

$$\mathcal{L}(\theta) = \mathbb{E}_{\mathbf{r} \sim |\psi_{\theta}|^2} [E_{\text{loc}}[\psi_{\theta}](\mathbf{r})]. \quad (4)$$

This means that, in practice, we alternate between sampling electron positions generated using a Langevin algorithm with the probability of the trial wavefunction

serving as the target distribution, and optimizing the trial wavefunction parameters using stochastic gradient descent. For further details, see Ref. [29].

### C. Computing excited states

We now introduce the central idea of this paper: a deep VMC method to compute the ground and low-lying excited states of a given electronic system. While we employ PauliNet to represent the individual wavefunctions, the method can also employ FermiNet or other real-space wavefunction representations with suitable modifications.

In a similar spirit to the ground-state optimization process, we first obtain a reasonable baseline for each state by performing a minimal state-averaged CASSCF calculation. This optimizes the energy average for all states in question and yields a single set of orbitals to construct each multi-determinant wavefunction, which are then supplemented by the analytically known cusp conditions. The choice of the CASSCF baseline ensures that the PauliNet ansatzes for the different excited states are close to orthogonal upon initialization. The Slater determinant coefficients  $c_p$  and linear coefficients  $c_{\mu k}$  of the single-electron orbitals  $\varphi_{\mu}(\mathbf{r}_i) = \sum_k c_{\mu k} \phi_k(\mathbf{r}_i)$  are both further optimized during the training process.

Our objective is to calculate the lowest  $n$  eigenstates of a given system, that is, find the set of orthogonal states that minimizes the energy expectation value. We approach this challenge by introducing a penalty term to the energy loss function (Eq. (4)) and optimizing the joint loss for  $n$  PauliNet instances:

$$\mathcal{L}(\theta) = \underbrace{\sum_i \mathbb{E}_i [E_{\text{loc}}[\psi_{\theta,i}(\mathbf{r})]]}_{\text{energy minimization}} + \alpha \underbrace{\sum_{i>j} \left( \frac{1}{1 - |S_{ij}|} - 1 \right)}_{\text{overlap penalty}}, \quad (5)$$

where  $\mathbb{E}_i = \mathbb{E}_{\mathbf{r} \sim |\psi_{\theta,i}|^2}$  and  $S_{ij}$  is the pairwise overlap between states  $i$  and  $j$ . The functional form of the overlap penalty is chosen to diverge when two states collapse and behave linearly when states are close to orthogonal. This allows states to overlap during the optimization procedure, while preventing their collapse and eventually driving them to orthogonality when they have settled in a local minimum of the energy. The hyperparameter  $\alpha$  weights the two loss terms and can be increased throughout the training to strengthen the orthogonality condition when approaching the final wavefunctions. For a sufficiently large  $\alpha$  the true minimum of the loss function corresponds to the sum of the energies of the lowest lying excited states. In practice a small  $\alpha$  is typically enough to drive the states towards orthogonality. To stabilize the training and reduce the computational cost we detach gradients in such a way that we only consider the overlap with the lower-lying states respectively, that is the ground state is subject to unconstrained energy minimization and the  $n$ -th excited state introduces

$n$  pairwise penalty terms. We compute the overlap of the unnormalized states  $i$  and  $j$  as the geometric mean of the two Monte Carlo estimates, obtained over distributions  $|\psi_{\theta,i}|^2$  and  $|\psi_{\theta,j}|^2$ , respectively:

$$S_{ij} = \text{sgn} \left( \mathbb{E}_i \left[ \frac{\psi_{\theta,j}(\mathbf{r})}{\psi_{\theta,i}(\mathbf{r})} \right] \right) \times \sqrt{\mathbb{E}_i \left[ \frac{\psi_{\theta,j}(\mathbf{r})}{\psi_{\theta,i}(\mathbf{r})} \right] \mathbb{E}_j \left[ \frac{\psi_{\theta,i}(\mathbf{r})}{\psi_{\theta,j}(\mathbf{r})} \right]}. \quad (6)$$

The sign of the overlap can be obtained from either of the two estimators, which match in the limit of infinite sampling. If the overlap is close to zero and the signs of the two estimates differ due to statistical noise of the sampling, we consider the states to be orthogonal. Similar to the energy loss, the gradient [39] of the pairwise overlap can be formulated such that it depends on the first derivative of the log wavefunction with respect to the parameters only (see Appendix A).

Finally, we note that different states may be modeled at different quality, which can lead to erroneous excitation energies. In order to improve the error cancellation of our ansatzes we employ a variance matching technique. As the variance of the energy  $\sigma^2$  can be considered a metric of how close a wavefunction is to a true eigenstate, variance matching procedures can be useful tools [23, 40, 41]. Here, we utilize a simple scheme: for single-state quantities such as total energies, we evaluate all wavefunctions at the end of training. For multi-state quantities, such as excitation energies or transition dipole moments, we match states of a similar variance. That is, if final  $\psi_{\theta,i}$  has a lower variance than final  $\psi_{\theta,j}$ , we take  $\psi_{\theta,i}$  at an earlier point in training. This simply involves computing  $\sigma^2$  of the training energies and applying exponential moving average at each iteration to monitor convergence. We find this procedure typically improves the final results.

## III. RESULTS

### A. Nearly exact solutions for small atoms and molecules

To demonstrate our method we start by applying it to a range of small atoms and molecules. We optimize the lowest lying excited states and compute their vertical excitation energies for the ground-state equilibrium geometry, with each PauliNet wavefunction containing a maximum of 10 determinants. In all of the systems we obtain highly accurate total energies and estimates of the first few excitation energies competitive with high-accuracy quantum chemistry methods.

In Fig. 1 the excitation energies of the lowest states are shown for several atoms. For all the atoms the energy of the first excited state is obtained within 2 mHa of the theoretical best estimate (TBE) [42]. Due to the high degree of symmetry the atoms exhibit degeneracies, that is multiple orthogonal states can be found corresponding

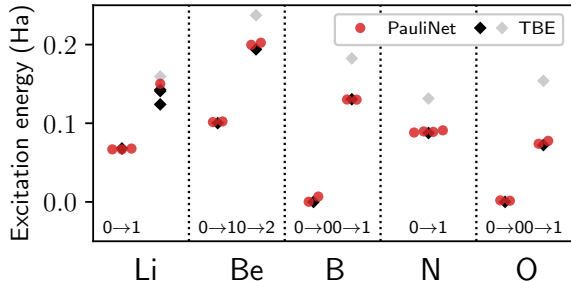


FIG. 1. **Deep VMC obtains highly accurate excited states for single elements.** PauliNet results (red) are compared to the theoretical best estimate (TBE) taken from the NIST database [42]. Multiple identical energies correspond to orthogonal degenerate states. To depict the gap with the following excited states grey diamonds give the next excitation energy respectively. For all the atoms we find the first excited state ( $0 \rightarrow 1$ ) with high accuracy. For Boron and Oxygen the ground state is threefold degenerate ( $0 \rightarrow 0$ ). For Li and Be a further excitation energy is found. While we can identify the second excited state in most systems, Li exhibits a cluster of multiple excited states with similar energies, and we cannot unambiguously assign the state found by excited PauliNet.

to the same energy, which is seen by multiple PauliNet results at the same energy level.

We then compute a larger number of excited states for LiH, BeH and Be. In each simulation we optimize eight ansatzes in parallel. In Fig. 2 we show the training process for the total energies as well as the convergence of the excitation energies. Based on the degeneracies we find a total of five (LiH), four (BeH) and three (Be) distinct excitation energies, respectively. Most excitation energies match excited states from references, and in particular we find that for all systems studied here we reliably find the first and except for one case the second excited states. However, especially for clusters of higher-lying excited states with similar energies, we typically do not find all members of the cluster. In these cases, the states found depend on the initialization of our ansatzes, as well as the total number of states that are being sought.

### B. Highly accurate wavefunctions: transition dipole moments and oscillator strengths

Total energies and vertical excitation energies are the primary focus when benchmarking excited-state methods as they are readily available from many theoretical models and provide a good initial guess of a particular method’s accuracy. However, they provide only a partial characterization of the electronic states, and while a method in question may give accurate energies, other quantities of key importance may be inaccurate [46–48].

Transition dipole moments (TDM) and oscillator strengths are two principal ground-to-excited transition

properties and are of great interest. TDMs determine how polarized electromagnetic radiation will interact with a system due to its distribution of charge, and therefore determine transition rates and probabilities of induced state changes. In the electric dipole approximation, the TDM between two states  $i$  and  $j$  is given by:

$$\mathbf{d}_{ij} = \langle \psi_i | \boldsymbol{\mu} | \psi_j \rangle, \quad (7)$$

where  $\boldsymbol{\mu} = \sum_k q \mathbf{r}_k$  is the sum over the position of each particle weighted by its charge, with  $q = -e$  for electronic systems. While the TDM is important for understanding a number of processes, including optical spectra, it is a complex vector quantity and not an experimental observable by itself. The closely related oscillator strength is what is inferred through experiment and is given by:

$$f_{ij} = \frac{2}{3} \Delta E d_{ij}^2, \quad (8)$$

where  $\Delta E$  is the excitation energy between states  $i$  and  $j$ , and  $d_{ij}^2$  is the dipole strength. It is known that, in addition to being more basis-set sensitive,  $d_{ij}$  and  $f$  are both highly dependent on the quality of the trial wavefunctions [49] and represent a more rigorous test for ab initio methods than just energies.

Recently, transition energies and oscillator strengths for a variety of small molecules have been computed using high-order CC calculations, systematically extrapolating to the complete basis set (CBS) limit, and comparing to experimental results where possible, in order to supply a comprehensive set of theoretical benchmarks [50, 51]. In that spirit, we now use these results to benchmark the accuracy of oscillator strengths computed using PauliNet. Furthermore, we also compare to multi-reference CC (MR-CC) results where possible [52]. We compute the first few electronic states for five molecules (BH,  $\text{CH}^+$ ,  $\text{H}_2\text{O}$ ,  $\text{NH}_3$ , CO), such that we obtain the first non-zero oscillator strength (within the dipole approximation) for each. All calculations [53] are performed at the same ground-state equilibrium geometries as Refs. [50, 51] and using the same number of determinants ( $\leq 10$ ) as in Section III A.

Our results for all systems are shown in Fig 3. First, we compute the amount of correlation energy recovered in the ground state, and find PauliNet matches high-order CC methods (upper panel). Second, we compute the excitation energy for each transition and find this to be close to the TBE, on par with CC and much more consistent than DFT where the accuracy depends on the molecule and on the exact DFT method used (central panel). Finally, we compare the oscillator strengths (for the  $0 \rightarrow 2$  transition) in the lower panel. Even high-order methods such as CC and MRCC can produce a spectrum of results depending on the expansion and basis set used, with this exacerbated in cheaper methods such as DFT (see the example of CO). In all systems, PauliNet compares well with experimental results, demonstrating the quality of deep VMC wavefunctions with just a minimal number of determinants.

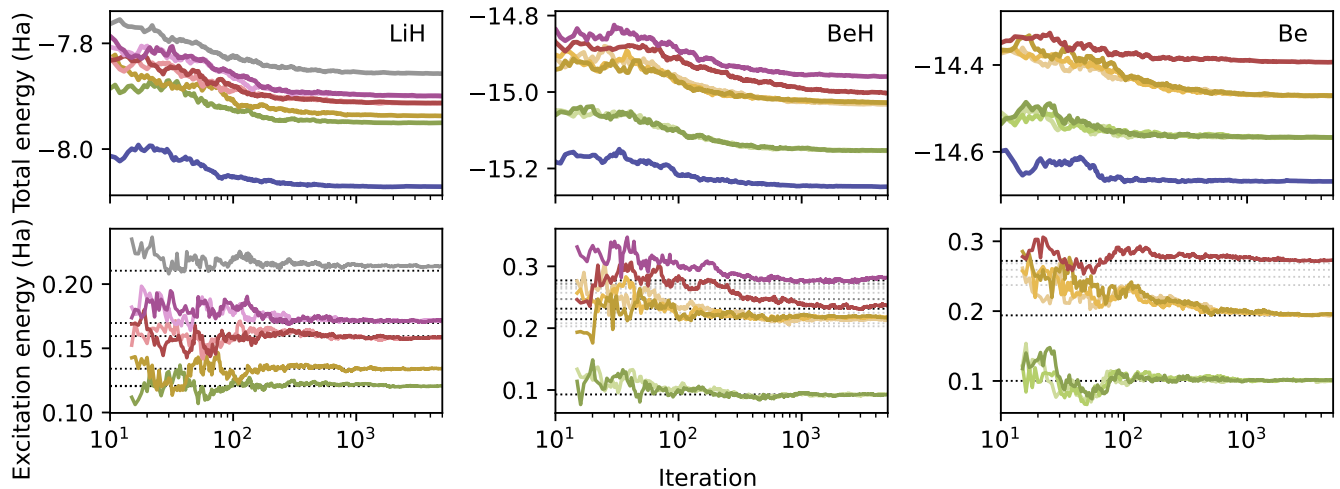


FIG. 2. **Optimizing low-lying excited states for small molecules.** Several excited states of LiH, BeH and Be are approximated. The convergence of the total energy (upper row) and the excitation energies (lower row) is shown. For degenerate states multiple ansatzes attain the same energy. Dotted horizontal lines are excitation energies from FCI calculations and other highly accurate references [43][44][45][42].

### C. Application to larger molecules

The previous two sections showed that we achieve highly accurate results across a range of small systems. While this is motivating, traditional high-accuracy methods that are better established are readily available for such small systems. In this section, to demonstrate the potential of excited PauliNet, we show that it can be applied in a straightforward manner to significantly larger molecules. For this objective, we choose the example of the benzene molecule (upper panel of Fig. 4). Studies of its electronic structure and other properties are plentiful due to its importance in bio and organic chemistry, and with 42 electrons it will be extremely demanding or even intractable for a high-level description of its electronic states, depending on the theory level used.

Using a slightly modified PauliNet ansatz with just 10 determinants, the same as in the much smaller systems, and slightly deeper neural networks we obtain very good total energies for the ground state and first excited state (left of Fig. 4). We note the better accuracy than much more demanding CC calculations, with this signifying highly accurate wavefunctions that can be used to compute other observables, as demonstrated in the previous section. The computed excitation energy is also shown (right of Fig. 4), with PauliNet giving comparable results to CC. In order to obtain the excitation energy we have again used the variance matching technique and averaged our results over wavefunctions at several training steps. This reduces dependencies on the hyperparameters of the variance matching, such as the smoothing parameter for the variances throughout the training process.

PauliNet formally scales as  $O(N^4)$  with number of

electrons  $N$ , and in practice we observe a scaling behavior  $O(N^3)$  for the systems investigated so far, which is related to quadratic scaling of the neural network with an extra factor from evaluation of the local energy. As PauliNet is currently implemented in a research code, which is not optimized for production purposes, the computational time will have a large prefactor which makes it computationally unfavorable to e.g. CC methods for small molecules. However, its very favorable scaling in  $N$  compared to  $O(N^{5-10})$  of high-level electronic structure methods dominates for larger molecules, and this is clearly visible in benzene. Table I compares the computational costs in terms of computing node hours of PauliNet and higher-order methods that have been used to obtain accurate Benzene ground-state energies. Although PauliNet is the computationally cheapest method – and in some cases by two orders of magnitude – it provides the best (variational) ground-state energy. As all methods compared in Fig. 4 provide similar excitation energies, these cannot be used to group the methods into more or less accurate, but overall this data indicates that PauliNet and deep VMC methods in general have a very favorable cost/accuracy trade-off for molecules of the size of benzene and beyond.

## IV. CONCLUSION

We have introduced an approach to compute highly accurate excited-state solutions of the electronic Schrödinger equation for molecules by using deep neural networks that are trained in an unsupervised manner with variational Monte Carlo. We have employed the PauliNet architecture [29] to approximate the ground-

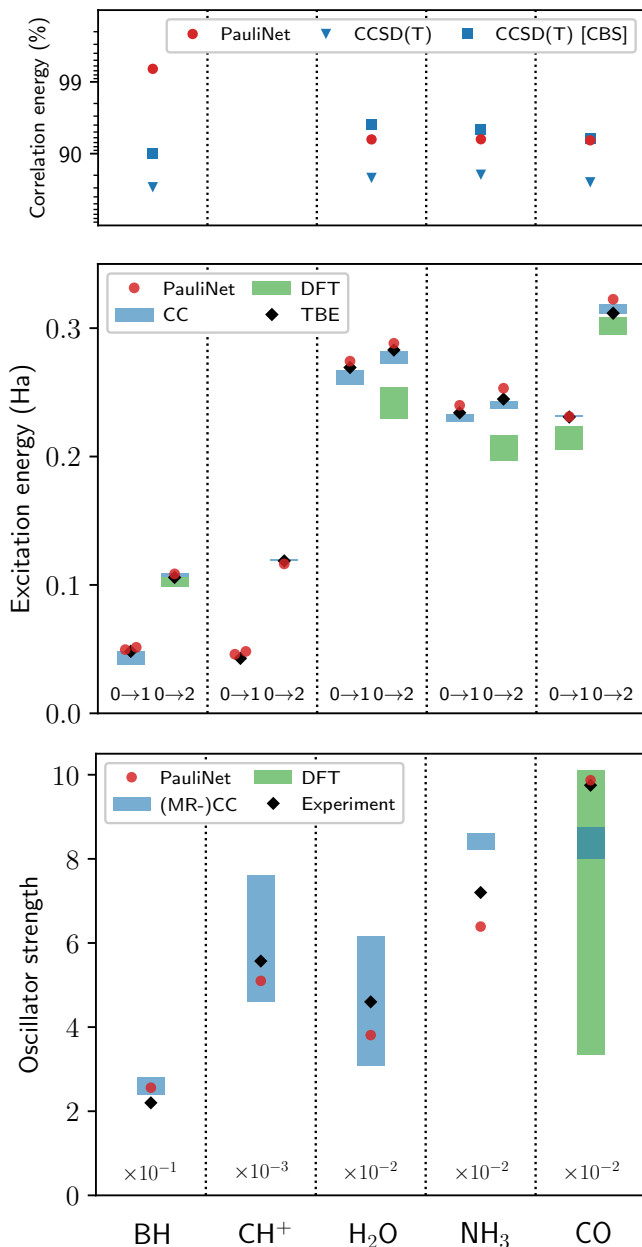


FIG. 3. **Deep VMC obtains highly accurate excited-state energies and wavefunctions for small molecules.** Upper panel: PauliNet recovers the same amount of correlation energy as high-order CC methods [42]. (CH<sup>+</sup>: No better reference energy to compare with.) Central panel: Lowest triplet (0→1) and singlet (0→2) excitation energies obtained using PauliNet, CC and DFT, with the TBE given. (BH and CH<sup>+</sup> exhibit degeneracy for the triplet state; CC is CCSD or higher, except for the triplet state of BH which includes CC2.) Lower panel: Oscillator strengths computed for the 0→2 transitions. PauliNet compares well to experiment in all systems and matches the accuracy of (MR-)CC results, demonstrating the quality of few-determinant PauliNet wavefunctions. (We have omitted a factor of two linked to degeneracy in BH and CO.) Refs: exact correlation energies [42, 54, 55]; excitation energies from CC [50–52, 56–59], DFT [58–61] and TBE [50, 51, 56, 62, 63]; oscillator strengths from (MR-)CC [50–52, 64, 65], DFT [66] and experiment [67–71].

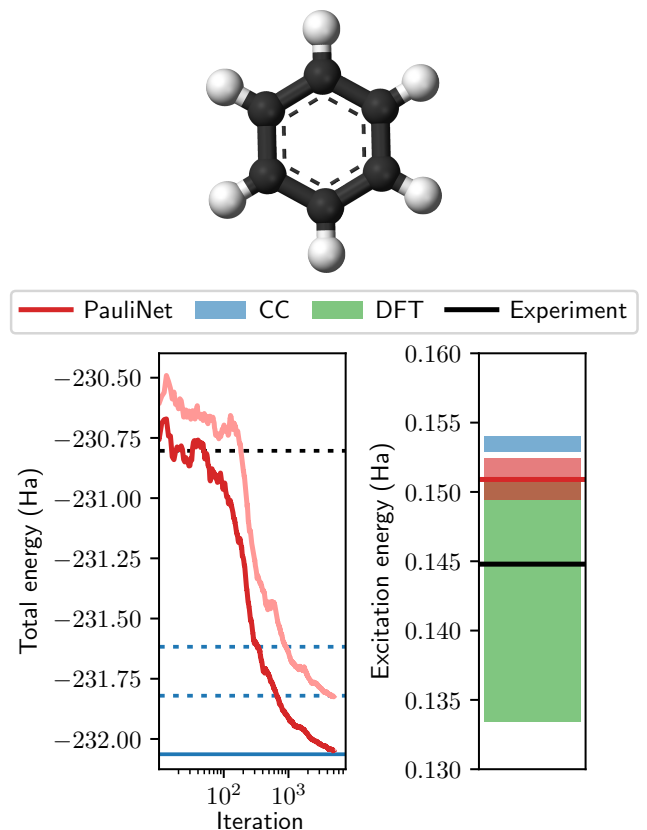


FIG. 4. **Calculating the two lowest electronic states of the benzene molecule.** Upper panel: benzene structure<sup>a</sup>. Left: Convergence of the total energy of the ground state (red) and excited state (light red) with training. Total energies of the ground state from HF at the CBS limit (dashed black), CCSD(T) in the frozen-core approximation with the aug-cc-pVnZ basis set ( $n = D, T$ ) (dashed blue), and full CCSD(T) at the CBS limit (solid blue) are shown [42]. Right: Excitation energy computed using PauliNet, DFT [61], CC [72] and Experiment [73].

<sup>a</sup> Reproduced from Wikipedia (credit to: Benjah-bmm27 / public domain)

TABLE I. **Computational cost for a single state.** PauliNet compared with state-of-the-art methods from Ref. [74] for a ground-state calculation of Benzene. Calculations in Ref. [74] used the cc-pVDZ basis. We achieve a significantly better total energy than all methods ( $\sim 0.45$  Ha lower) at a fraction of the cost on a single GPU. N.B. We have converted their core hours to node hours for comparison purposes.

Method	Node hours
PauliNet	$2.5 \times 10^2$
CCSDTQ	$6.9 \times 10^2$
AS-FCIQMC	$1.5 \times 10^3$
DMRG	$2.2 - 2.9 \times 10^3$
FCCR	$2.5 \times 10^3$
MBE-FCI	$4.7 \times 10^4$

and excited-state wavefunctions, however other architectures such as FermiNet [30] or second quantization approaches [31] could also be employed, with suitable modifications. As our approach to find excited states only constrains the excited-state wavefunctions, the ability to compute highly accurate and variational absolute ground-state energies is unchanged. In addition, we demonstrate for a number of small molecules up to 42 electrons, that excited PauliNet can reliably find the first excitation energies with an accuracy that is on par with high-level electronic structure methods, whereas cheaper methods such as DFT are less consistent in approximating these energies. The accuracy of the excited-state wavefunctions is underlined by an accurate match of oscillator strengths, which depend on the transition dipole moment, a quantity that is more sensitive to the exact form of the wavefunction than the energy. For benzene (42 electrons), PauliNet already requires significantly less computational time than higher-order methods, and this advantage will only improve for larger molecules. Formally, a single PauliNet is an  $\mathcal{O}(N^4)$  method for  $N$  electrons, due to the computational cost of the Hartree-Fock or CASSCF baseline, however in practice we see that the determinant computation is the computational bottleneck for the system sizes tested, and we therefore currently have empirically an  $\mathcal{O}(N^3)$  dependency. In addition, for excited-state calculations  $n$  PauliNet replicas are used which gives rise to  $\mathcal{O}(nN^3)$ .

Notably, almost identical excited PauliNet architectures are used across the systems shown in this paper – up to minor modifications such as the budget of Slater determinants and the total number of excited states requested, and a deeper network for benzene to adapt for a potentially more complex wavefunction. Whereas a skilled quantum chemist can usually tune and specialize an existing electronic structure method to give very high-accuracy results for a given molecule, our aim is the exact opposite: to provide a method that, by leveraging

machine learning tools, is as automated as possible and will work over a wide range of Hamiltonians provided.

By combining the present approach with recent and ongoing extensions of PauliNet [34] and FermiNet [35] that variationally compute entire potential energy surfaces, both highly accurate ground- and excited-state energy surfaces are now accessible with deep VMC methods. This could be used in order to compute conical intersections, barrier crossing upon photoexcitation and other interesting processes where molecular dynamics interacts with excited states.

One of the limitations of the current approach is that it appears difficult to reliably find all excited states up to a given desired number, especially in cases where several excited states have similar energies. This is a complex problem which depends on the Hartree-Fock/CASSCF initialization, on the total number of states requested, on the learning algorithm and the expressiveness of the architecture and will be studied in more detail elsewhere. However the first excited state could be reliably found for all molecules studied here, and apart from one exception also the second excited state. This, in combination with the high numerical accuracy and the favorable computational cost, makes deep VMC a promising method to compute both ground- and excited-state properties for small- and medium-sized molecules with dozens or even low hundreds of electrons.

## ACKNOWLEDGMENTS

We thank Tim Gould (Griffith U) for early discussions about variational principles for excited states. Funding is gratefully acknowledged from the Berlin mathematics center MATH+ (Projects AA1-6, AA2-8), European Commission (ERC CoG 772230), Deutsche Forschungsgemeinschaft (NO825/3-2), and the Berlin Institute for Foundations in Learning and Data (BIFOLD).

- 
- [1] R. Lindh and L. González, *Quantum Chemistry and Dynamics of Excited States: Methods and Applications* (John Wiley & Sons, 2020).
  - [2] W. Kohn and L. J. Sham, Phys. Rev. **140**, A1133 (1965).
  - [3] E. Runge and E. K. U. Gross, Phys. Rev. Lett. **52**, 997 (1984).
  - [4] P. Elliott, J. I. Fuks, A. Rubio, and N. T. Maitra, Phys. Rev. Lett. **109**, 266404 (2012).
  - [5] J. I. Fuks, K. Luo, E. D. Sandoval, and N. T. Maitra, Phys. Rev. Lett. **114**, 183002 (2015).
  - [6] Y. Suzuki, L. Lacombe, K. Watanabe, and N. T. Maitra, Phys. Rev. Lett. **119**, 263401 (2017).
  - [7] N. Singh, P. Elliott, T. Nautiyal, J. K. Dewhurst, and S. Sharma, Phys. Rev. B **99**, 035151 (2019).
  - [8] N. T. Maitra, Journal of Physics: Condensed Matter **29**, 423001 (2017).
  - [9] C. A. Ullrich and I. V. Tokatly, Phys. Rev. B **73**, 235102 (2006).
  - [10] P. G. Szalay, T. Müller, G. Gidofalvi, H. Lischka, and R. Shepard, Chemical Reviews **112**, 108 (2012).
  - [11] K. Sneskov and O. Christiansen, WIREs Computational Molecular Science **2**, 566, <https://wires.onlinelibrary.wiley.com/doi/pdf/10.1002/wcms.99>.
  - [12] FCI scales exponentially, while truncated CI scales polynomially.
  - [13] The scaling of CC depends on the particular method used: CC2  $\mathcal{O}(N^5)$ , CCSD  $\mathcal{O}(N^6)$ , CCSD(T)  $\mathcal{O}(N^7)$ , CC3  $\mathcal{O}(N^7)$ , CCSDT  $\mathcal{O}(N^8)$ , CCSDT(Q)  $\mathcal{O}(N^9)$ , CCSDTQ  $\mathcal{O}(N^{10})$ .
  - [14] W. M. C. Foulkes, L. Mitas, R. J. Needs, and G. Rajagopal, Rev. Mod. Phys. **73**, 33 (2001).
  - [15] K. T. Williams, Y. Yao, J. Li, L. Chen, H. Shi, M. Motta, C. Niu, U. Ray, S. Guo, R. J. Anderson, J. Li, L. N. Tran, C.-N. Yeh, B. Mussard, S. Sharma, F. Bruneval, M. van Schilfegaarde, G. H. Booth, G. K.-L. Chan, S. Zhang, E. Gull, D. Zgid, A. Millis, C. J. Umrigar, and L. K. Wag-



- ner (Simons Collaboration on the Many-Electron Problem), *Phys. Rev. X* **10**, 011041 (2020).
- [16] M. A. Morales, J. McMinis, B. K. Clark, J. Kim, and G. E. Scuseria, *Journal of Chemical Theory and Computation* **8**, 2181 (2012).
- [17] A. Benali, K. Gasperich, K. D. Jordan, T. Applencourt, Y. Luo, M. C. Bennett, J. T. Krogel, L. Shulenburger, P. R. C. Kent, P.-F. Loos, A. Scemama, and M. Caffarel, *The Journal of Chemical Physics* **153**, 184111 (2020), <https://doi.org/10.1063/5.0021036>.
- [18] B. M. Austin, D. Y. Zubarev, and W. A. Lester, *Chemical Reviews* **112**, 263 (2012).
- [19] D. M. Ceperley and B. Bernu, *The Journal of Chemical Physics* **89**, 6316 (1988), <https://doi.org/10.1063/1.455398>.
- [20] N. S. Blunt, S. D. Smart, G. H. Booth, and A. Alavi, *The Journal of Chemical Physics* **143**, 134117 (2015), <https://aip.scitation.org/doi/pdf/10.1063/1.4932595>.
- [21] R. Send, O. Valsson, and C. Filippi, *Journal of Chemical Theory and Computation* **7**, 444 (2011).
- [22] M. Dash, J. Feldt, S. Moroni, A. Scemama, and C. Filippi, *Journal of Chemical Theory and Computation* **15**, 4896 (2019).
- [23] S. D. Pineda Flores and E. Neuscamman, *The Journal of Physical Chemistry A* **123**, 1487 (2019).
- [24] L. Zhao and E. Neuscamman, *Journal of Chemical Theory and Computation* **12**, 3436 (2016).
- [25] J. A. R. Shea and E. Neuscamman, *Journal of Chemical Theory and Computation* **13**, 6078 (2017).
- [26] N. S. Blunt and E. Neuscamman, *Journal of Chemical Theory and Computation* **15**, 178 (2019).
- [27] K. Choo, G. Carleo, N. Regnault, and T. Neupert, *Phys. Rev. Lett.* **121**, 167204 (2018).
- [28] S. Pathak, B. Busemeyer, J. N. B. Rodrigues, and L. K. Wagner, *The Journal of Chemical Physics* **154**, 034101 (2021).
- [29] J. Hermann, Z. Schätzle, and F. Noé, *Nature Chemistry* **12**, 891 (2020).
- [30] D. Pfau, J. S. Spencer, A. G. D. G. Matthews, and W. M. C. Foulkes, *Phys. Rev. Research* **2**, 033429 (2020).
- [31] K. Choo, A. Mezzacapo, and G. Carleo, *Nat. Commun.* **11**, 2368.
- [32] J. Han, L. Zhang, and W. E, *J. Comput. Phys.* **399**, 108929 (2019).
- [33] J. S. Spencer, D. Pfau, A. Botev, and W. M. C. Foulkes, *arXiv:2011.07125 [physics.comp-ph]* (2021).
- [34] M. Scherbela, R. Reisenhofer, L. Gerard, P. Marquetand, and P. Grohs, *arXiv:2105.08351v2 [physics.comp-ph]* (2021).
- [35] S. G. Nicholas Gao, *arXiv:2110.05064v2 [cs.LG]* (2021).
- [36] G. Carleo and M. Troyer, *Science* **355**, 602 (2017).
- [37] J. Westermayr and P. Marquetand, *Chemical Reviews* **121**, 9873 (2021).
- [38] Z. Schätzle, J. Hermann, and F. Noé, *The Journal of Chemical Physics* **154**, 124108 (2021), <https://doi.org/10.1063/5.0032836>.
- [39] We employ gradient clipping to stabilize the training.
- [40] L. Otis, I. Craig, and E. Neuscamman, *The Journal of Chemical Physics* **153**, 234105 (2020), <https://doi.org/10.1063/5.0024572>.
- [41] P. J. Robinson, S. D. Pineda Flores, and E. Neuscamman, *The Journal of Chemical Physics* **147**, 164114 (2017), <https://doi.org/10.1063/1.5008743>.
- [42] R. D. J. III, NIST Computational Chemistry Comparison and Benchmark Database, NIST Standard Reference Database Number 101 (2021).
- [43] A. Bande, H. Nakashima, and H. Nakatsuji, *Chemical Physics Letters* **496**, 347 (2010).
- [44] P. Jasik, J. E. Sienkiewicz, J. Domsta, and N. E. Henriksen, *Phys. Chem. Chem. Phys.* **19**, 19777 (2017).
- [45] J. Pitarch-Ruiz, J. Sánchez-Marín, and A. M. Velasco, *Journal of Computational Chemistry* **29**, 523 (2008).
- [46] E. Brémond, M. Savarese, C. Adamo, and D. Jacquemin, *Journal of Chemical Theory and Computation* **14**, 3715 (2018).
- [47] A. Tajti and P. G. Szalay, *Journal of Chemical Theory and Computation* **15**, 5523 (2019).
- [48] A. Tajti, L. Tulipán, and P. G. Szalay, *Journal of Chemical Theory and Computation* **16**, 468 (2020).
- [49] R. Crossley, *Physica Scripta* **T8**, 117 (1984).
- [50] P.-F. Loos, A. Scemama, A. Blondel, Y. Garniron, M. Caffarel, and D. Jacquemin, *Journal of Chemical Theory and Computation* **14**, 4360 (2018), pMID: 29966098, <https://doi.org/10.1021/acs.jctc.8b00406>.
- [51] A. Chrayteh, A. Blondel, P.-F. Loos, and D. Jacquemin, *Journal of Chemical Theory and Computation* **17**, 416 (2021), pMID: 33256412, <https://doi.org/10.1021/acs.jctc.0c01111>.
- [52] D. Bhattacharya, N. Vaval, and S. Pal, *The Journal of Chemical Physics* **138**, 094108 (2013), <https://doi.org/10.1063/1.4793277>.
- [53]  $\text{CH}^+$  was not included in the CC calculations in Refs. [50, 51]. We instead compare to (MR-)CC results in Ref. [52], using the same ground-state equilibrium geometry, which was obtained in a split valence basis augmented with diffuse and polarization functions. See Refs. [52, 63] for more details.
- [54] D. P. O'eill and P. M. W. G. \*, *Molecular Physics* **103**, 763 (2005), <https://doi.org/10.1080/00268970512331339323>.
- [55] E. Giner, D. Traore, B. Pradines, and J. Toulouse, *The Journal of Chemical Physics* **155**, 044109 (2021), <https://doi.org/10.1063/5.0057957>.
- [56] H. Larsen, K. Hald, J. Olsen, and P. Jørgensen, *The Journal of Chemical Physics* **115**, 3015 (2001), <https://doi.org/10.1063/1.1386415>.
- [57] K. Kowalski and P. Piecuch, *Chemical Physics Letters* **347**, 237 (2001).
- [58] P. Cronstrand, B. Jansik, D. Jonsson, Y. Luo, and H. Ågren, *The Journal of Chemical Physics* **121**, 9239 (2004), <https://doi.org/10.1063/1.1804175>.
- [59] P. Salek, T. Helgaker, O. Vahtras, H. Ågren, D. Jonsson, and J. Gauss, *Molecular Physics* **103**, 439 (2005), <https://doi.org/10.1080/00268970412331319254>.
- [60] F. Liu, Z. Gan, Y. Shao, C.-P. Hsu, A. Dreuw, M. Head-Gordon, B. T. Miller, B. R. Brooks, J.-G. Yu, T. R. Furlani, and J. Kong, *Molecular Physics* **108**, 2791 (2010), <https://doi.org/10.1080/00268976.2010.526642>.
- [61] C. Adamo, G. E. Scuseria, and V. Barone, *The Journal of Chemical Physics* **111**, 2889 (1999), <https://doi.org/10.1063/1.479571>.
- [62] Z. Biglari, A. Shayesteh, and A. Maghari, *Computational and Theoretical Chemistry* **1047**, 22 (2014).
- [63] J. Olsen, A. M. De Meías, H. J. A. Jensen, and P. Jørgensen, *Chemical Physics Letters* **154**, 380 (1989).
- [64] M. Barysz, *Theoretica chimica acta* **90**, 257 (1995).



- [65] J. R. Lane, V. Vaida, and H. G. Kjaergaard, The Journal of Chemical Physics **128**, 034302 (2008), <https://doi.org/10.1063/1.2814163>.
- [66] Y. Tawada, T. Tsuneda, S. Yanagisawa, T. Yanai, and K. Hirao, The Journal of Chemical Physics **120**, 8425 (2004), <https://doi.org/10.1063/1.1688752>.
- [67] C. H. Douglass, H. H. Nelson, and J. K. Rice, The Journal of Chemical Physics **90**, 6940 (1989), <https://doi.org/10.1063/1.456269>.
- [68] B. Mahan and A. O’Keefe, Astrophysical Journal **248** (1981).
- [69] P. A. Thorn, M. J. Brunger, P. J. O. Teubner, N. Diakomichalis, T. Maddern, M. A. Bolorizadeh, W. R. Newell, H. Kato, M. Hoshino, H. Tanaka, H. Cho, and Y.-K. Kim, The Journal of Chemical Physics **126**, 064306 (2007), <https://doi.org/10.1063/1.2434166>.
- [70] T. Chen, Y.-W. Liu, X.-J. Du, Y.-C. Xu, and L.-F. Zhu, The Journal of Chemical Physics **150**, 064311 (2019), <https://doi.org/10.1063/1.5083933>.
- [71] X. Kang, Y. W. Liu, L. Q. Xu, D. D. Ni, K. Yang, N. Hirao, K. D. Tsuei, and L. F. Zhu, The Astrophysical Journal **807**, 96 (2015).
- [72] P.-F. Loos, F. Lipparini, M. Boggio-Pasqua, A. Scemama, and D. Jacquemin, Journal of Chemical Theory and Computation **16**, 1711 (2020), pMID: 31986042, <https://doi.org/10.1021/acs.jctc.9b01216>.
- [73] J. P. Doering, The Journal of Chemical Physics **51**, 2866 (1969).
- [74] J. J. Eriksen, T. A. Anderson, J. E. Deustua, K. Ghanem, D. Hait, M. R. Hoffmann, S. Lee, D. S. Levine, I. Magoulas, J. Shen, N. M. Tubman, K. B. Whaley, E. Xu, Y. Yao, N. Zhang, A. Alavi, G. K.-L. Chan, M. Head-Gordon, W. Liu, P. Piecuch, S. Sharma, S. L. Ten-no, C. J. Umrigar, and J. Gauss, The Journal of Physical Chemistry Letters **11**, 8922 (2020), pMID: 33022176, <https://doi.org/10.1021/acs.jpclett.0c02621>.

## Appendix A: Gradient of the loss function

In order to differentiate the loss function we explicitly formulate the gradient. We consider the general case of a mixed observable:

$$O_{ij} = \text{sgn} \left( \mathbb{E}_i \left[ \frac{O\psi_{\theta,j}(\mathbf{r})}{\psi_{\theta,i}(\mathbf{r})} \right] \right) \times \sqrt{\mathbb{E}_i \left[ \frac{O\psi_{\theta,j}(\mathbf{r})}{\psi_{\theta,i}(\mathbf{r})} \right] \mathbb{E}_j \left[ \frac{O\psi_{\theta,i}(\mathbf{r})}{\psi_{\theta,j}(\mathbf{r})} \right]}. \quad (\text{A1})$$

This expression reduces to the pairwise overlaps (Eq. (6)) upon setting  $O = \text{Id}$ . The derivative of this term can be expressed as:

$$\partial O_{ij} = \frac{1}{2O_{ij}} \left\{ \left( \mathbb{E}_i \left[ \left( \frac{O\psi_{\theta,i}(\mathbf{r})}{\psi_{\theta,j}(\mathbf{r})} - \mathbb{E}_i \left[ \frac{O\psi_{\theta,j}(\mathbf{r})}{\psi_{\theta,i}(\mathbf{r})} \right] \right) \right] \right. \right. \\ \left. \left. \partial \ln |\psi_{\theta,i}(\mathbf{r})| \right] \times \mathbb{E}_i \left[ \frac{O\psi_{\theta,j}(\mathbf{r})}{\psi_{\theta,i}(\mathbf{r})} \right] + (i \iff j) \right\}. \quad (\text{A2})$$

Considering the Hamilton operator  $H$  and setting  $i = j$  we recover the gradient of the energy loss [29]:

$$\partial E_{ii} = 2\mathbb{E}_i \left[ \frac{H\psi_{\theta,i}(\mathbf{r})}{\psi_{\theta,i}(\mathbf{r})} - \mathbb{E}_i \left[ \frac{H\psi_{\theta,i}(\mathbf{r})}{\psi_{\theta,i}(\mathbf{r})} \right] \right] \partial \ln |\psi_{\theta,i}(\mathbf{r})|. \quad (\text{A3})$$

## Appendix B: Hyperparameters

TABLE II. Hyperparameters used in numerical calculations. (See Ref. [29] for more details.)

Hyperparameter	Value
One-electron basis	6-311G
Maximum number of determinants	10
Dimension of $\mathbf{e}$ (# distance features)	32
Dimension of $\mathbf{x}_i$ (embedding dimension)	128
Dimension of $\mathbf{z}_i$ (kernel dimension)	64
Number of interaction layers L	4
Number of layers in $\eta_{\theta}$	3
Number of layers in $\kappa_{\theta}$	3
Number of layers in $\mathbf{w}_{\theta}$	1
Number of layers in $\mathbf{h}_{\theta}$	2
Number of layers in $\mathbf{g}_{\theta}$	2
Batch size	2000
Number of walkers	1000
Number of equilibration steps	500
Number of training steps:	
small-systems	5000
intermediate-systems	20000
benzene	5000
Optimizer	AdamW
Learning rate scheduler	CyclicLR
Minimum/maximum learning rate	0.0001/0.005
Cyclic frequency	500
Clipping window q	5
Minimum/maximum $\alpha$	0.5/2.0
Epoch size	10
Resampling frequency	3
Number of decorrelation sampling steps	5
Target acceptance	57%